Journal of Science and Transport Technology
Journal homepage: https://jstt.vn/index.php/en

UNIVERSITY OF TRANSPORT TECHNOLOGY

Development and Evaluation of DUT Vibro: A High-Precision Vibrating Wire Sensor Readout

Van-Lam Cao[1], Dinh-Viet Le[2], Duc-Chau Le[1,*]
[1]Faculty of Road and Bridge Engineering, The University of Danang – University of Science and Technology, Danang City, Vietnam
[2]Kumoh National Institute of Technology, Gumi City, Korea

Article info
Type of article:
Original research paper

DOI:
https://doi.org/10.58845/jstt.utt.2025.en.5.3.25-43

***Corresponding author:**
Email address:
ldchau@dut.udn.vn

Received: 14/04/2025
Received in Revised Form: 13/06/2025
Accepted: 03/07/2025

Abstract: This study presents the development and evaluation process of a vibrating wire sensor readout named DUT Vibro, with both hardware and software entirely developed by Vietnamese researchers. The primary objective of this paper is to evaluate the efficacy of two methods to determine the resonant frequency of the vibrating wire to facilitate precise strain calculations. In this study, parabolic interpolation is investigated to improve the accuracy of the resonant frequency of a steel wire, addressing the limitation of Fast Fourier Transform (FFT) constrained by the storage capacity of the microcontroller. In addition, the determined resonant frequency of DUT Vibro is compared with a commercial DIGIANGLE (DAS). Furthermore, two stimulation signals—sine and square waves—were employed to compare their impact on measurement accuracy. The results indicate that the parabolic interpolation method yields the lowest standard deviation, closely aligning with the DAS readout, and demonstrates stability across both low and high load conditions. In contrast, the FFT method exhibits greater error variability, particularly in the medium load range, due to the influence of noise and non-linearities in the response signal. The sine wave stimulus combined with parabolic interpolation achieves the highest accuracy. The measurement system maintains high linearity, with linearity errors below 0.5% of full scale (FS), and the lowest linearity error is 0.129% FS when using a sine wave stimulus. Linear regression analysis reveals a slope coefficient of approximately 0.052, reflecting a linear relationship between load and measured strain. Based on these findings, the parabolic interpolation method has been integrated into the DUT Vibro readout, meeting stringent accuracy requirements for strain measurement applications.
Keywords: vibrating wire sensor, fast fourier transform, parabolic, linearity.

1. Introduction

Vibrating wire sensors have played a critical role in the field of monitoring and structural health assessment for large-scale civil engineering projects, such as bridges, dams, nuclear power plants, and other infrastructure facilities. This technology has been widely adopted and extensively studied by researchers worldwide. Dunnicliff's [1] seminal work laid the theoretical and practical foundations for strain measurement using vibrating wire sensors, focusing on monitoring foundation and structural deformations [2-9]. Zhao et al. [3] investigated a single-coil vibrating wire sensor data acquisition system employing the

STM32F103 microcontroller to generate low-voltage PWM signals, excite the vibrating wire through frequency sweeping, and measure frequency via amplification, filtering, and signal normalization modules. Their system demonstrated reliable performance coefficients. Hua-Ling et al. [4] developed a high-precision vibration signal acquisition system based on vibrating wire sensors and the STM32 microcontroller, incorporating storage functionality to enhance safety in engineering construction. The system supported signal acquisition, data storage on SD cards, and real-time monitoring through computer connectivity across multiple points. Mei et al. [5] explored the response of the steel wire in vibrating wire sensors when the excitation coil was positioned at different position and excited using various signal types, aiming to improve sensor performance. Theoretical and experimental analyses were conducted to identify optimal excitation modes, enhancing excitation efficiency and mitigating the influence of higher-order resonant frequencies. This finding suggest that precise coil positioning and tailored signal inputs could stabilize frequency readouts under varying load conditions, directly relevant to improving the reliability of vibrating wire sensor systems. Fu et al. [6] designed a bridge vibration monitoring device utilizing vibrating wire sensors as the primary sensing elements. The system integrated a microcontroller with ZigBee and GPRS technologies for wireless data collection and transmission to a server. Tao et al. [7] proposed a novel method for dynamic stress measurement using vibrating wire sensors, overcoming the limitations of traditional methods suited only for static measurements. This approach employed adaptive dynamic frequency excitation to sustain continuous wire oscillation without attenuation, combined with a spectral interpolation algorithm based on the Fourier transform to accurately determine the resonant frequency. The results demonstrated a theoretical error of only 0.015 Hz and a sampling rate of up to 325 Hz, validating the method's efficacy and feasibility. Tao and his colleagues demonstrated the effective suppression of higher-order resonant interference and achieving precise dynamic stress measurements. These results provide critical strategies for enhancing frequency estimation accuracy in complex, time-varying loading conditions. Sang et al. [8] introduced a fast frequency sweep method to measure the resonant frequency of vibrating wire sensors using the STM32 microcontroller. The method involved two excitation steps: an initial coarse frequency estimation followed by precise measurement. Leveraging the STM32's high clock pulse, this approach reduced errors and enhanced measurement accuracy. Hou et al. [9] presented a distributed bridge health monitoring system employing LoRa technology to improve real-time performance, efficiency, and automation compared to traditional systems. The system comprised data acquisition nodes, relay nodes, and a central node, built on the STM32H7 microcontroller paired with the SX1268 radio frequency chip. The results confirmed the system's ability to meet real-time monitoring requirements, effectively supporting bridge maintenance and risk warning operations.

Recent research often focuses on developing sensor readout using STM32 microcontrollers, which offer high performance at a lower cost compared to other high-end microcontroller families. In addition, Fast Fourier Transform (FFT) algorithms are commonly embedded in microcontrollers to compute the resonant frequency of sensors in real time, enabling the derivation of strain values and timely data transmission to processing systems. Most studies utilize square wave signals for stimulation phase and perform FFT analysis on the response signal. However, few investigations have explored the impact of transitioning from square wave to sine wave excitation.

A notable contribution is the work of Tao et al. [7], which proposed a phase-compensated self-adaptive excitation method to shorten excitation time. Following FFT analysis, the authors applied resonant frequency interpolation to enhance accuracy and reduce processing time during response signal acquisition. However, this method required establishing the relationship between excitation frequency and corresponding phase offset. Upon detecting the rising (or falling) edge of the oscillation signal, the system supplied a high (or low) voltage level with the corresponding phase as the excitation signal. This relationship was stored in a look-up table derived from prior experiments across various resonant frequencies, accelerating the measurement process.

In this study, the authors developed a vibrating wire sensor readout with functionalities comparable to global counterparts, utilizing the STM32 microcontroller series to optimize manufacturing costs. A key distinction of the device is its ability to employ both sine and square wave excitations. The Cooley-Tukey FFT algorithm [10] was implemented to compute the resonant frequency in real time, combined with a three-point parabolic interpolation method to enhance the accuracy of the results. Unlike Tao et al. [7], a logarithmic frequency sweep was applied during the stimulation phase to control excitation time while ensuring the frequency range aligns with the sensor's characteristics, accurately determining the resonant frequency of steel wire.

The paper is structured as follows: Section 2 outlines the theoretical foundations of vibrating wire sensors, FFT, and the parabolic interpolation method using three points. Section 3 describes the development process of the DUT Vibro vibrating wire sensor readout. Section 4 presents the experimental validation of the developed readout. Section 5 discusses the research findings. Section 6 summarizes the finding contributions and future works.

2. Literature Review

2.1. Vibrating wire sensor

The vibrating wire sensor is a sensor comprising a steel tube housing a fine steel wire. The tube is surrounded by one or two magnetic inductive coils and includes a thermistor [1]. Both ends of the steel tube are securely fixed to supports, which are connected to other mechanical components. The steel wire, the primary sensitive element of the sensor, is held under tension at both ends by the supports from the point of manufacture. The detailed structure of this sensor is illustrated in Fig. 1. When the structure to which the sensor is attached is subjected to loading, the surface undergoes deformation, causing the supports to shift and altering the tension of the steel wire. A magnetic inductive coil, positioned proximate to the wire, is responsible for exciting oscillations and capturing the response signal. The operation of the vibrating wire sensor is divided into two primary phases: Stimulation Phase and the Response Phase.

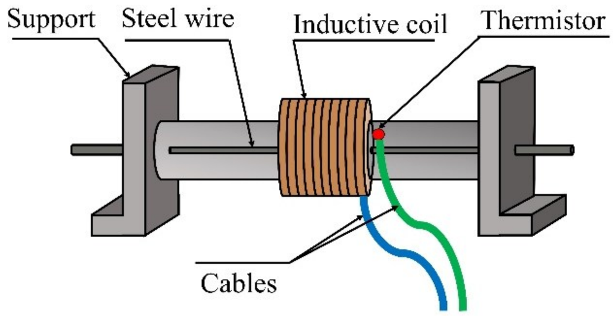

Fig. 1. Schematic of virating wire sensor

During the Stimulation Phase, an electrical pulse is transmitted to the coil, inducing the steel wire to oscillate due to the influence of the magnetic field. This pulse typically takes the form of a square or sine wave, adjusted within the frequency range specified by the manufacturer. A sine wave is smooth and single-frequency, while a square wave switches abruptly and contains multiple harmonics. Each type of excitation wave has its own advantages and limitations; therefore, both sine and square waves are investigated in this study to propose the most optimal excitation method for the vibrating wire sensor. In addition, two excitation methods are employed: linear frequency sweeping and logarithmic frequency sweeping. Fig. 2 depicts the excitation process using a sine wave with linear frequency sweeping, while Fig. 3 illustrates the sine wave excitation with logarithmic frequency sweeping.

The Linear Frequency Sweep method (Fig. 2) employs an excitation signal that linearly sweeps frequencies from 10 Hz to 10,000 Hz over 1 second, with the frequency increasing uniformly over time. The signal has an amplitude ranging from -1.0 to 1.0, and the Fast Fourier Transform (FFT) spectrum reveals a nearly uniform amplitude distribution within the 450–6000 Hz range [11], sharply declining beyond 10,000 Hz. This method evenly covers the entire frequency range, making it suitable for identifying resonant frequencies across a broad spectrum.

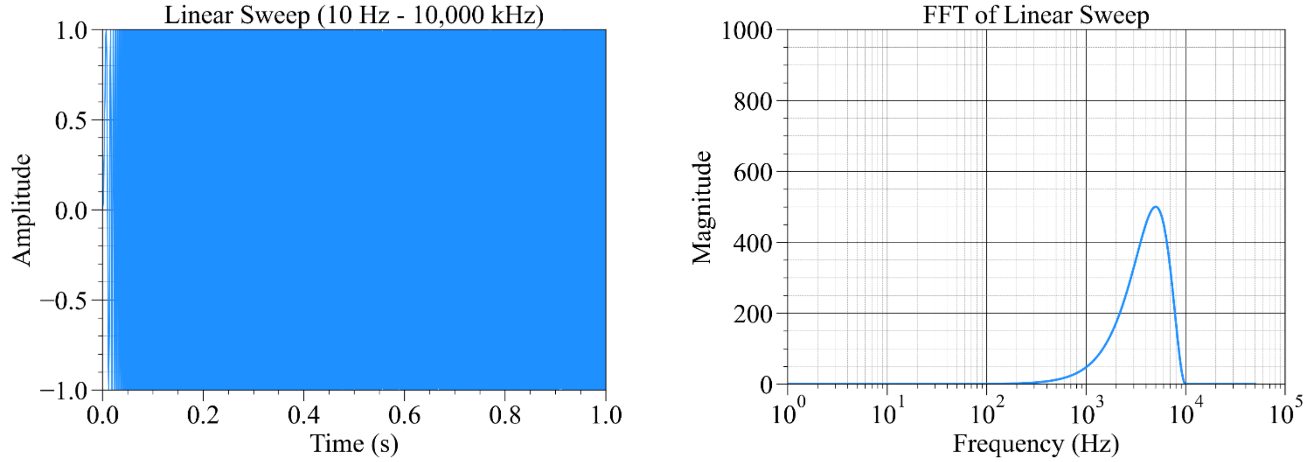

(a) (b)

Fig. 2. Linear sweep stimulation method: (a) Excitation signal, (b) FFT plot

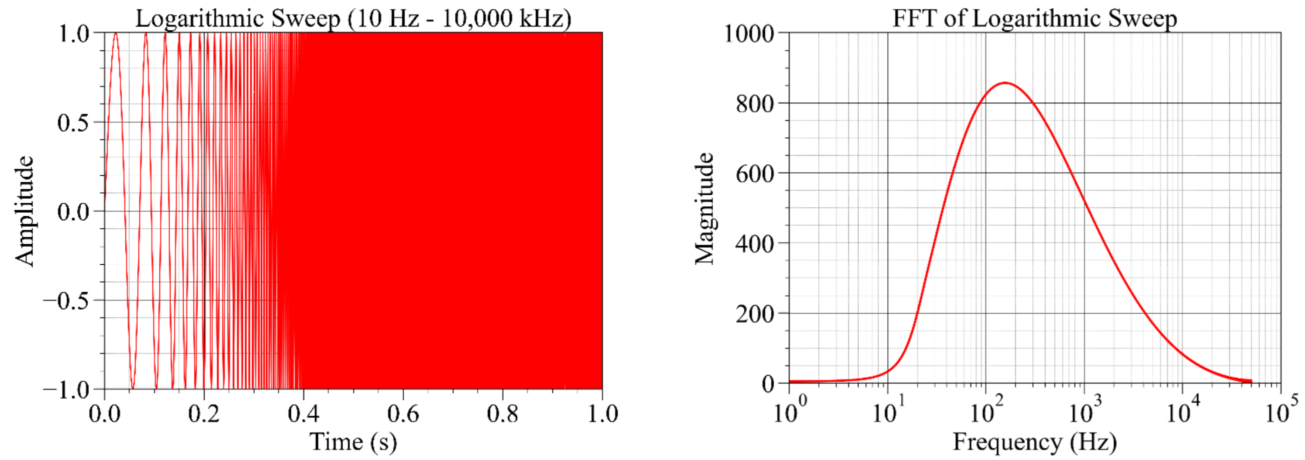

(a) (b)

Fig. 3. Logarithmic sweep stimulation method: (a) Excitation signal, (b) FFT plot

The Logarithmic Frequency Sweep method (Fig. 3) also sweeps frequencies from 10 Hz to 10,000 Hz over 1 second, but follows a logarithmic scale, where the frequency increases rapidly at the start and slows toward the end. The signal maintains an amplitude from -1.0 to 1.0, and the FFT spectrum shows a peak amplitude (approximately 800) at 1,000 Hz, concentrating energy at lower frequencies where the resonant frequency of vibrating wire sensors typically occurs.

Generally, the Logarithmic Frequency Sweep method is preferred for exciting steel wire in the vibrating wire sensors due to its superior control over excitation time. By allocating more time to lower frequencies (below 1,000 Hz), where the sensor's resonant frequency is commonly located, this method enhances resolution and sensitivity in the critical frequency range, enabling precise determination of the resonant frequency of steel wire. In contrast, the Linear Frequency Sweep method distributes time equally across all frequencies, potentially reducing resolution at lower frequencies and increasing excitation time.

Consequently, the Logarithmic Frequency Sweep is the optimal choice for allocating more excitation time to lower frequency bands where resonance is expected and improving accuracy in measuring the resonant frequency of vibrating wire sensors.

When the frequency of the electrical pulse approaches the natural frequency of the steel wire, resonance occurs. During the Response Phase, the steel wire oscillates stably at its natural frequency, but energy dissipation occurs due to factors such as: internal damping, air resistance and friction. As a result, the steel wire is oscillation to decay over time, resulting in a gradually decreasing amplitude. This process induces a magnetic effect, generating a periodic response signal with diminishing amplitude, which is recorded by the reading signal module. The reading module picks up the voltage induced in the coil due to the motion of the steel wire. Fig. 4 illustrates the two primary phases of the vibrating wire sensor: Stimulation Phase and the Response Phase.

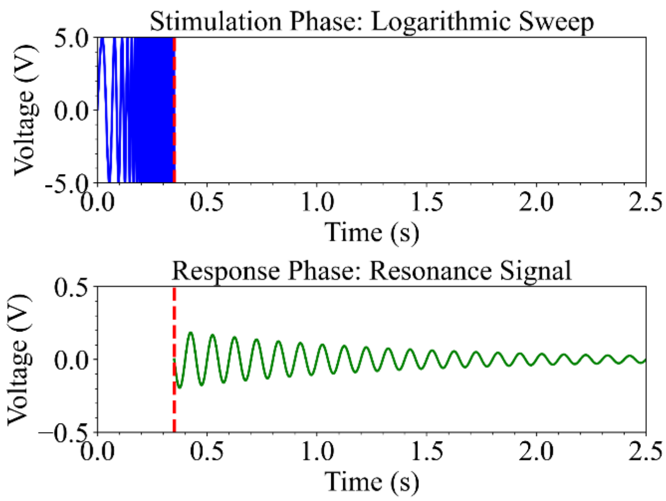

Fig. 4. Description of Stimulation Phase and Response Phase

The signal from the vibrating wire sensor is processed through amplification and noise-filtering circuits, followed by FFT analysis to determine the oscillation frequency. The frequency corresponding to the highest amplitude in the FFT spectrum represents the natural frequency of the steel wire. Changes in loading alter the tension of the steel wire, resulting in variations in its natural frequency.

In addition, environmental temperature affects the natural frequency of the vibrating wire in the sensor, causing thermal expansion during long-term monitoring. Therefore, a thermistor is integrated into the sensor to measure temperature enabling output corrections. Temperature is determined based on the relationship between the measured resistance and the manufacturer's provided temperature lookup table.

Currently, vibrating wire sensors are widely applied in various monitoring devices in the construction industry, including strain gauges, rock bolt stress sensors, elongation measurement tools, shotcrete stress sensors, crack monitoring devices, and pore water pressure piezometers [2-9].

2.2. Fast Fourier Transfer

The Fast Fourier Transform (FFT) is an efficient algorithm for computing the Discrete Fourier Transform (DFT), enabling the frequency spectrum analysis of a signal. In vibrating wire sensor readout, the FFT is employed to determine the natural frequency of the steel wire within the sensor by processing the voltage signal acquired from an Analog-to-Digital Converter (ADC).

The fundamental formula for the DFT of a signal sequence $x(n)$ with length N is expressed as:

$$X(k)=\sum_{n=0}^{N-1}x(n)e^{-j2\pi kn/N},\quad k=0,1,\ldots,N-1 \tag{1}$$

where $X(n)$ represents the frequency spectrum at the frequency index k.

In practice, the input signal often contains noise due to environmental factors or limitations of the measurement equipment. To mitigate the effects of noise and spectral leakage, the input signal is typically multiplied by the Hanning window function, defined as follows:

$$w(n)=\frac{1}{2}\left(1-\cos\left(\frac{2\pi n}{N-1}\right)\right) \tag{2}$$

The signal, after the application of the Hanning window function [7,12], is expressed as follows:

$$x_w(n) = x(n)\cdot w(n) \tag{3}$$

Consequently, Equation (1) for the DFT of the input signal, after applying the window function, is rewritten as follows:

$$X(k) = \sum_{n=0}^{N-1} x_w(n) e^{-j2\pi kn/N}, \quad k = 0,1,\ldots,N-1 \tag{4}$$

Typically, FFT is embedded in the hardware of readout, where memory and processing speed are constrained. Consequently, the Cooley-Tukey algorithm [10] is commonly employed to compute the signal's frequency, reducing computational complexity. Furthermore, this algorithm performs calculations directly without requiring auxiliary arrays for intermediate results, making it well-suited for embedded programming on resource-limited hardware. According to this algorithm, the signal is assumed to have a length N that is a power of 2, and the signal sequence is divided into two parts: samples with even indices (n=2m) and samples with odd indices (n=2m+1). The DFT can then be expressed as follows:

$$\begin{cases} X\left(k + \frac{N}{2}\right) = E(k) + W_N^k \cdot O(k) \\ W_N^k = e^{-j\frac{2\pi}{n}kn} \end{cases} \tag{5}$$

where E(k) and O(k) are the DFTs of the even and odd sequences, respectively. This process is repeated recursively until the DFTs are reduced to base cases of length 2, resulting in an overall complexity of O(NlogN).

2.3. Parabolic interpolation using three points

In embedded systems employing microcontrollers, particularly those with limited memory such as the STM32F103C8T6 [13], the implementation of digital signal processing algorithms requires a careful balance between accuracy and computational cost. When performing the FFT for signal spectrum analysis, the peak frequency often does not align with the discrete frequency bins provided by the FFT. However, increasing the FFT size to enhance frequency resolution is infeasible due to SRAM memory constraints. Consequently, the three-point parabolic interpolation method is adopted as an alternative solution to reduce the number of computations and conserve memory.

Let A_{k-1}; A_k; and A_{k+1} denote the amplitudes of three adjacent FFT bins, where A(k) is the maximum value among the three points, corresponding to the frequency $f_0(k)$ (as shown in Fig. 5). It is assumed that these three points lie on a parabola described by the following equation:

$$A(f) = a \times f^2 + b \times f + c \tag{6}$$

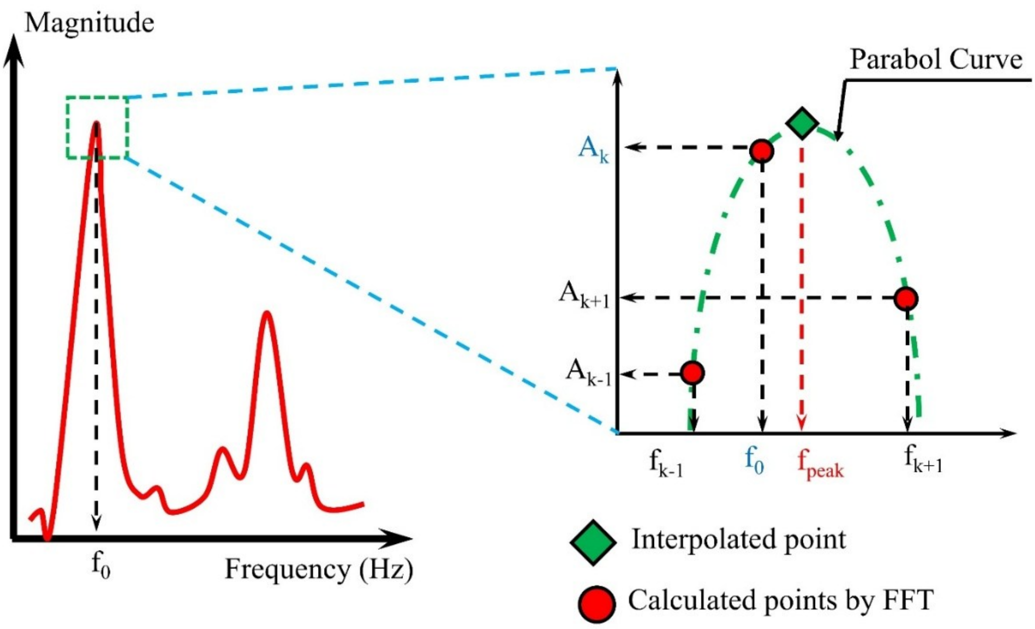

Fig. 5. Description of Parabolic interpolation using three points

Consequently, the actual peak frequency is determined through three-point parabolic interpolation as follows:

$$f_{peak} = f_0 + \frac{A_{k-1} - A_{k+1}}{2\left(A_{k-1} - 2A_k + A_{k+1}\right)} \times \Delta f \tag{7}$$

where Δf is the frequency resolution, calculated by dividing the sampling frequency f_s by the number of input signal samples N. This method derives from finding the extremum of a quadratic function through its derivative and can be executed rapidly with simple arithmetic operations, making it suitable for real-time computations.

3. Design of Vibrating Wire Sensor Readout

3.1. Stimulation circuit

In vibrating wire sensor readout, the stimulation module plays a critical role in generating a controlled electrical signal—typically a sine or square wave—to mechanically stimulate the sensor's wire (Fig. 6). The objective of this signal is to induce short-term forced oscillations, thereby producing free oscillations that enable the determination of the wire's characteristic resonant frequency, which depends on mechanical stress and ambient environmental conditions. According to the sensor manufacturer's recommendations, the excitation frequency range for all types of vibrating wire sensors spans from 450 Hz to 6,000 Hz [11]. In this study, two excitation signal types—sine and square waves—are employed. The logarithmic frequency sweep method is adapted because it efficiently scans a wide frequency range by exponentially increasing frequencies, allowing faster coverage than a linear sweep. It also adjusts sweep timing to prioritize critical frequencies, ensuring timely and accurate capture of the sensor's feedback signal.

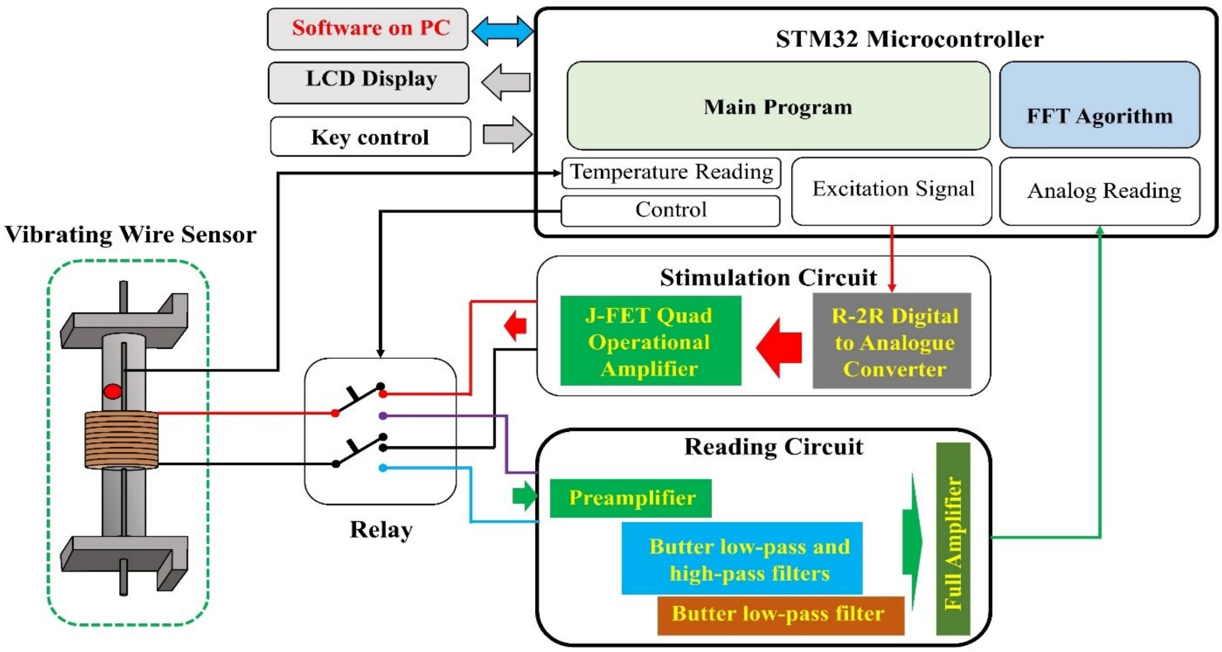

Fig. 6. Flowchart of Virating wire sensor readout DUT Vibro

In the design of this module, an STM32 microcontroller is utilized to generate an 8-bit parallel digital signal via eight GPIO pins [13]. These signals are fed into a digital-to-analog converter (DAC) implemented as an R-2R resistor network, producing a continuous analog voltage corresponding to each binary input value. The R-2R resistor network is a widely used DAC technique due to its simplicity, ease of implementation, and high linearity when low-tolerance resistors are employed. The output voltage of the R-2R network is calculated using the following formula:

$$V_{out} = V_{ref} \cdot \sum_{k=0}^{7} \left(\frac{b_k}{2^{8-k}} \right) \tag{8}$$

where $b_k \in \{0,1\}$ represents the k-th bit in the 8-bit data sequence and V_{ref} is the reference voltage of

3.3 V, and V_{out} is the analog output voltage, varying from 0 to V_{ref}.

The binary data is continuously updated based on a lookup table pre-stored in the program memory of the STM32 microcontroller. This table contains discrete values representing one cycle of a sine or square wave. Updating the data at a high rate (typically from a few kHz to tens of kHz) enables the generation of an analog signal that closely approximates a continuous waveform. Although the output signal from the R-2R DAC achieves high linearity, it remains confined to the positive domain, lacking a negative component. To produce a symmetrical alternating current (AC) signal centered around 0 V—essential for accurately inducing mechanical oscillations—the system incorporates an analog signal processing stage using a JFET Quad Operational Amplifier (Op-Amp). The JFET Op-Amp is selected for its high input impedance and low noise characteristics, which minimize signal errors while ensuring robust performance for waveforms with frequencies ranging from hundreds of Hz to tens of kHz, aligning with the excitation frequency range of the vibrating wire sensor.

In this processing stage, the DAC output is fed into an operational amplifier circuit configured for level shifting and gain amplification. The objective is to convert the DAC's output voltage from the range [0, V_{ref}] to a symmetrical range of peak voltage [$-V_p$, $+V_p$] centered around 0 V. This conversion process is described by the following equation:

$$V_{AC}(t) = A \times \left(V_{out}(t) - \frac{V_{ref}}{2} \right) \tag{9}$$

where: A is a tunable gain factor determined by the op-amp circuit, which can be adjusted via a potentiometer connected to the control terminals of the op-amp.

3.2. Reading Circuit

During the development of the measurement system utilizing vibrating wire sensors, one of the major technical challenges encountered was the processing of weak and noise-sensitive signals from the sensor. After the sensor is excited by a stimulation signal, the STM32 microcontroller assumes the coordination role by controlling a relay to switch the connection state, thereby routing the two signal wires from the sensor to the reading circuit.

The signal obtained at the sensor output has a very low amplitude, typically in the range of a few millivolts, and commonly appears as a damped oscillation—a characteristic feature of vibrating wire sensors [1]. The frequency of this wave typically includes the natural resonant frequency range of the vibrating wire and noises, within the excitation wave range of 450 Hz to 6000 Hz. However, this very nature also renders the signal highly susceptible to electromagnetic interference and unwanted frequency components present in the measurement environment. Consequently, there is a critical need for a robust signal processing system that not only amplifies the signal but also effectively filters out noise and preserves signal integrity throughout the entire processing chain.

To overcome this issue, we designed a signal processing chain composed of multiple functionally coordinated blocks (Fig. 6). The chain begins with a primary amplification stage employing high-precision differential op-amps, enabling signal amplitude to be increased by over 5000 times while maintaining linearity. Subsequently, the signal is passed through second-order Butterworth high-pass and low-pass filters to effectively eliminate noise components outside the frequency band of interest.

After filtering and amplification, the signal cannot be directly fed into the microcontroller due to its incompatible waveform characteristics. Therefore, the signal is further processed to shift its voltage range into the 0 to 3.3 V domain. Due to the need to immediately determine the resonant frequency of the vibrating wire, selecting the number of samples is critical as it affects the chip's memory. Moreover, the Cooley-Tukey FFT algorithm used in this study requires the number of signal samples to be a power of two. Therefore, the signal sample size is set to 1024 samples, with the sampling frequency at the maximum sampling rate of the STM32F103C8T6 chip, corresponding to 512 FFT points since the FFT result is symmetrical. This signal undergoes FFT analysis, followed by parabolic interpolation to accurately identify the resonant frequency of the vibrating wire. In addition, the vibrating wire sensor integrates an NTC (Negative Temperature Coefficient) thermistor connected in series with a fixed resistor under a 3.3 V supply. The voltage drop across this resistor is measured via another analog input of the STM32, from which the ambient temperature around the sensor is computed using a manufacturer-provided resistance-to-temperature lookup table. The resolution of measured temperature is 0.1 °C. The final results — including the peak resonant frequency and temperature — are displayed in real-time on the LCD screen.

3.3. Vibrating wire sensor readout DUT-Vibro

The vibrating wire sensor readout, designated as DUT-Vibro, was developed using the STM32F103C8T6 microcontroller (Fig. 7). The STM32F103C8T6 [13] is a high-performance microcontroller from the STM32F1 series by STMicroelectronics, based on the ARM Cortex-M3 architecture and operating at clock speeds up to 72 MHz. It features 64 KB of Flash memory, 20 KB of RAM, and a wide range of integrated peripherals including a 12-bit ADC, timers, UART, SPI, I2C interfaces, and USB connectivity. Due to its efficient processing capabilities, low power consumption, and cost-effectiveness, the STM32F103C8T6 is widely used in embedded systems requiring precise control and real-time data processing. These characteristics make it especially suitable for sensor signal acquisition and measurement applications, as demonstrated in this study.

The DUT-Vibro readout is operated via two control buttons and is equipped with a display for real-time measurement output. The yellow button (on the left) is used to initiate the measurement mode for vibrating wire sensors, while the other button (on the right) allows for switching the input signal source, enabling compatibility with other sensor types when system expansion is required.

Upon pressing the yellow button, the readout activates a relay to enter the excitation mode, generating oscillations for the sensor. After a predefined duration, the relay automatically switches to the reading mode to capture the sensor's response signal. This signal is then processed using FFT followed by parabolic interpolation to precisely identify the resonant frequency of steel wire in the sensor. The final resonant frequency along with the temperature value (measured via the thermistor in the sensor) is then displayed on the LCD screen.

The DUT-Vibro readout is also equipped with two communication ports: one dedicated to firmware updates and the other for connecting to a computer for interaction with control software. Additionally, the power supply system is designed to support both battery operation and standard 220V AC. This dual-mode capability ensures that the device can be reliably deployed in a variety of settings, from controlled laboratory environments to field measurement applications. Furthermore, the video tutorials for using the DUT Vibro device have been released on Mendeley Data [14].

Fig. 7. Vibrating wire sensor readout DUT Vibro

3.4. Software

Both embedded firmware and PC-based control software were developed as part of this study. The embedded firmware, programmed into the DUT-Vibro readout, is responsible for processing input commands from the control buttons, activating the relay to trigger the excitation signal, and subsequently switching to the signal acquisition mode. Signal processing algorithms, including the FFT and parabolic interpolation, are integrated directly into the firmware to calculate the resonance frequency in real time. After calculating the resonant frequency value, the temperature is determined based on the voltage value read by the analog pin of the STM32 microcontroller. The resulting frequency and temperature data are displayed on LCD screen.

Furthermore, the firmware is designed with multitasking capabilities, allowing it to receive control commands from both physical buttons and the PC-based software via a USB interface. During measurement, the STM32 firmware transmits raw signal data (1024 samples) and real-time FFT results (512 points) to PC software via asynchronous UART at 9,600 bps. This burst transmission, buffered for efficient packet delivery, enables storage and detailed analysis of the vibrating wire sensor's resonant frequency and temperature data.

The PC-based control software is designed with a graphical user interface based on C# language, allowing users to send measurement commands and select appropriate measurement modes to the DUT-Vibro readout (Fig. 8). These modes are tailored to common excitation frequency ranges that correspond to various types of vibrating wire sensors, ensuring optimal measurement accuracy.

During the measurement process, raw signal data and FFT results from the embedded firmware in the DUT-Vibro device are transmitted directly to the PC via a USB connection. The control software then displays both the time-domain signal and its corresponding FFT spectrum in real time, providing users with immediate visual feedback. Furthermore, the software enables users to export both datasets in CSV format for advanced analysis and post-processing.

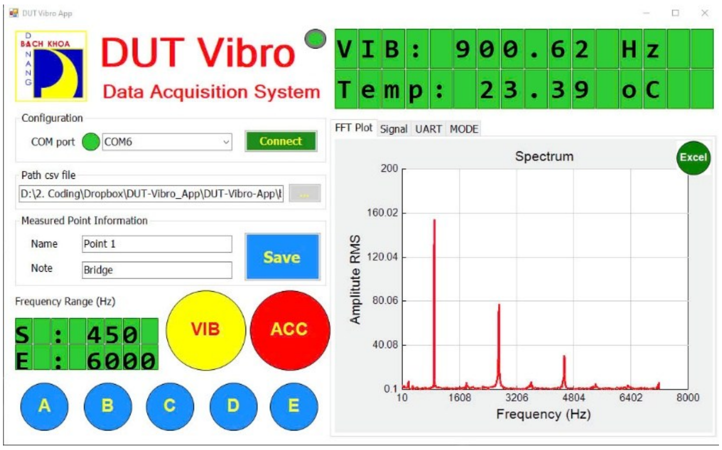

Fig. 8. Controller software for data acquisition

4. Experiment to Validate the Performance of the DUT-Vibro Readout

4.1. Experimental Steel Beam Model

The steel beam model was designed to simulate the real working conditions of a flexural beam, thereby enabling assessment of the strain measurement system's accuracy and reliability (Fig. 9). The overall structure consists of a steel beam mounted within a rigid steel frame, ensuring structural stability during load application.

The steel frame serves as a support structure and has a rectangular shape with a width of 600 mm and a height of 300 mm. It is constructed from high-strength structural steel to ensure the required stiffness and stability during testing. Two high-strength steel supports are mounted on the frame, spaced at a fixed distance of 375 mm—corresponding to the effective span length of the beam. Each support is 205 mm in height and is securely bolted to the frame's base to prevent any displacement throughout the load application process. On the left side of the frame, a movable clamp is installed to securely fix one end of the beam, forming a rigidly clamped boundary condition (analogous to a fixed support in structural models). This configuration ensures that the end of the beam does not rotate or slide under applied loads and accurately simulates common boundary conditions such as the clamped–pinned beam model.

The steel beam used in the experiment has an overall length of 560 mm, which is longer than the span between the two supports to ensure both ends are properly and securely supported. The beam has a rectangular cross-section with a width of 38 mm and a thickness of 5 mm, providing a slender profile conducive to observable deformation under loading. The beam is constructed from CT-3 steel, a widely structural steel in construction, valued for its excellent machinability, moderate strength, and elastic properties ideal for deformation verification.

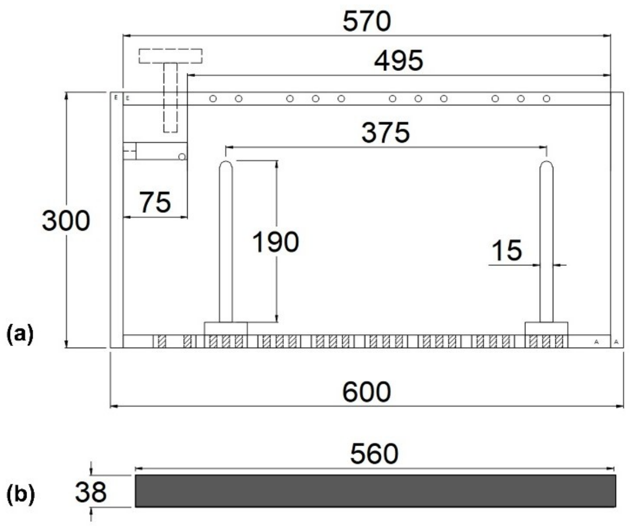

Fig. 9. Description of the experimental steel frame and beam: (a) Steel frame and supports; (b) Steel beam

4.2. Test equipments

In this verification experiment, the GV-2405 vibrating wire strain gauge, manufactured by Geovan (South Korea), was selected for use [11]. This specialized sensor is designed with a gauge length of 150 mm between its two mounting points, ensuring high accuracy in measuring oscillations in structural components such as steel beams. The sensor's structure includes a magnetic induction coil that functions to both excite the vibrating wire and receive the response signal. This configuration ensures the GV-2405's full compatibility with the DUT-Vibro readout, designed specifically for processing signals from single-coil vibrating wire sensors.

Additionally, the sensor is equipped with an integrated thermistor to measure the ambient temperature at the installation location. This temperature data is intended to support frequency correction, as temperature variations can affect wire tension and thus shift the sensor's natural frequency. The GV-2405 provides four signal wires in total: two for the vibration signal (related to the induction coil) and two for temperature signal transmission from the thermistor.

However, in the scope of this verification test, temperature compensation was omitted to simplify the data processing procedure, as the experiment was conducted over a short duration in a controlled laboratory environment where temperature effects were considered negligible. The focus was instead placed on evaluating the fundamental performance of the DUT-Vibro readout.

To ensure measurement reliability, the GV-2405 sensor was securely mounted at the mid-span of the steel beam using epoxy adhesive – a high-strength bonding material with excellent mechanical resistance. The installation was carefully executed to prevent sensor displacement during the experiment, minimizing measurement error caused by unintended vibrations or loosened attachments. The beam's mid-span was chosen as the installation point because it undergoes the greatest deformation under load, thereby allowing the sensor to effectively capture the relevant dynamic response characteristics.

The DIGIANGLE-NO-VW (DAS), South Korea vibrating wire sensor readout [15] is employed to evaluate the resonant frequency measurements of the GV-2405 sensor. This commercial device excites the sensor's single-coil wire using a plucked excitation method, delivering a square excitation voltage to induce stable vibrations within the 400 Hz to 6000 Hz range for all sensors. The device can simultaneously read three channels from vibrating wire sensors, making it highly suitable for applications in measuring strain, stress, water pressure, and displacement in construction projects, bridges, dams, tunnels, and foundations. The DAS operates with a rechargeable lithium battery (500mAh, 3.7V), providing continuous operation for over 10 hours and is easily recharged via an integrated USB port.

The DAS device support multiple reading modes to various vibrating wire sensor types, ensuring compatibility across diverse applications. MODE [A] displays frequency in Hz (450–6000 Hz) for standard sensors, while MODE [B] outputs kHz^2 (1200–3500 Hz) for load sensors and piezometers. MODES [C] and [D] (450–1000 Hz) apply factory-supplied constants of 4.062 and 3.304, respectively, to convert kHz^2 to microstrain for surface-mounted and underground sensors. MODE [E] uses a constant of 0.39102 (1000–3500 Hz) for spot-welded sensors, yielding microstrain. These precalibrated constants, derived from manufacturer specifications, ensure accurate conversion of squared frequency to engineering units, enhancing measurement reliability.

To evaluate the DUT-Vibro readout's performance in detecting the resonant frequency of vibrating wire sensors under real-world conditions, an experiment was conducted using the GV-2405 sensor. The DUT-Vibro internally generates sinusoidal and square wave excitation signals, alternately applied with a ±5 V amplitude and 150-ms duration within the 450–6000 Hz range, to assess their impact on frequency measurement accuracy. Sinusoidal waves minimize harmonic distortion, enhancing signal clarity for precise frequency detection, while square waves, rich in harmonics, test robustness against noise. This internal excitation simplifies system complexity by eliminating external hardware with results validated against the DAS readout [15]. In each measurement, the DUT-Vibro readout collects raw data directly from the sensor through the integrated signal processing circuit. This data includes both time-domain signals and FFT-processed signals, which are transmitted and stored in *.csv file format via the control software on a computer. Storing the data in CSV format facilitates subsequent processing and analysis, while allowing for the use of common analysis tools such as MATLAB, Python, or Excel for visualization and further processing. In addition to storing FFT spectrum data, the DUT-Vibro device performs resonance frequency interpolation using a three-point parabolic algorithm. The resonance frequency obtained from this interpolation, along with the value derived from the original FFT spectrum, is saved for future quantitative evaluation. During the analysis phase, the resonance frequency values measured by DUT-Vibro and its standard deviation will be compared with measurements from a commercial DAS device with verified accuracy, which serves as the reference device. By comparing the error between the two devices at various load levels, the relative accuracy, repeatability, and reliability of the DUT-Vibro in acquiring and processing signals from the vibrating wire sensor can be assessed.

During the verification experiment procedure, loading plates were used to apply varying load levels to the steel beam, causing mechanical deformation in the vibrating wire sensor. The load was applied concentrically at the midpoint of the beam, which is the location of maximum internal force in a simply supported beam. Load increments were controlled and applied in specific steps with weights of: 0 g (no load), 716 g, 964 g, 2249 g, 2783 g, 3499 g, 4557 g, and 5090 g. These load levels were selected to produce a diverse range of strain profiles, enabling more accurate evaluation of the sensor's response under various working conditions.

At each load level, the sensor signal was measured three times consecutively. This repetition minimizes the impact of random measurement errors, increasing the reliability of the results. Each measurement provides a corresponding resonance frequency value, reflecting the actual deformation state of the vibrating wire sensor under load. Monitoring the change in resonance frequency with varying load allows the relationship between strain in the wire and the electrical signal to be evaluated, which is essential for analyzing the effectiveness of the signal processing techniques employed in the measurement system.

In this experiment, both the DAS and DUT-Vibro readouts were used in parallel to evaluate measurement performance. The two devices were connected alternately to the same vibrating wire sensor, operating under identical loading and environmental conditions to ensure consistency and objectivity in the comparison of results. Each readout performed three measurements for each load level to minimize the effect of errors in the measurement process. The data collected from both devices was recorded, and then analyzed by load level to assess the deviation, stability, and reliability between the two devices. In this process, the DUT-Vibro device employed a three-point parabolic interpolation algorithm to determine the resonance frequency from the signal spectrum. The main objective of the experiment was not only to validate the functionality of the DUT-Vibro device but also to evaluate the effectiveness of the interpolation method integrated into the signal processing. The experimental results will provide the scientific basis to determine the potential application of the DUT-Vibro device in practical scenarios.

5. Results and Discussions

The resonance frequency results of the vibrating wire in the sensor from the DAS readout, calculated using the FFT method and the three-point parabolic interpolation method, are presented in Figs. 10 and 11 for the sine and square wave stimulation methods, respectively. Additionally, the specific values of the resonance frequency and the standard deviation, with the DAS readout values taken as reference, are summarized in Table 1. DAS readout is a common commercial vibrating wire sensor readout in Vietnam that has been verified by an independent institute in Korea before the manufacturer commercialized this product.

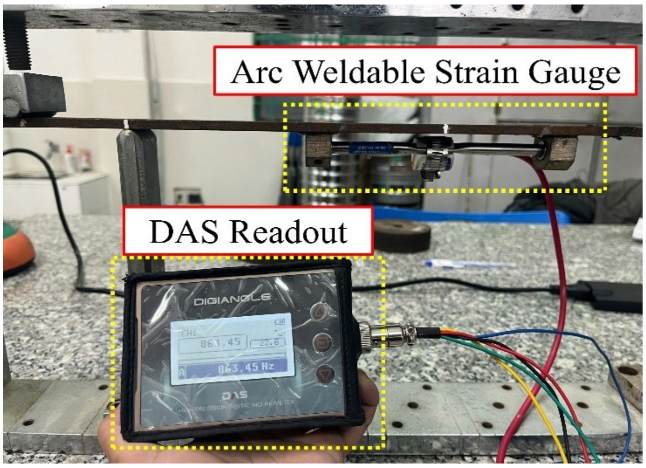

Fig. 10. DAS readout and Arc Weldable Strain Gauge GV2405 sensor

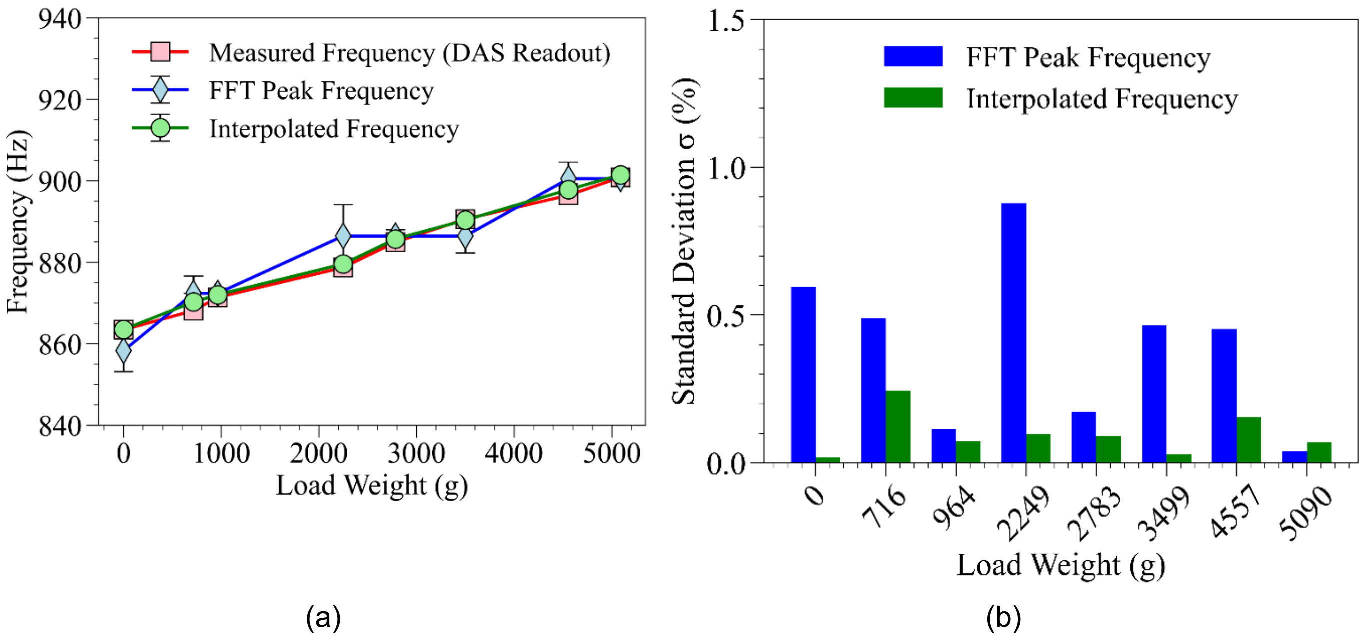

Fig. 11. Comparison of DAS readout, FFT peak, and interpolated frequencies using Sine wave stimulus: (a) Resonant frequencies vs. Load weight; (b) Frequency deviation vs. Load weight

Table 1. Statistical analysis of resonant frequencies and standard deviations

Load weigth (g)	DASPeak Frequency (Hz)	Sine wave stimulus				Square wave stimulus			
		FFT		Parabolic interpolation		FFT		Parabolic interpolation	
		$f_0(Hz)$	Std (%)	$f_{peak}(Hz)$	Std (%)	$f_0(Hz)$	Std (%)	$f_{peak}(Hz)$	Std (%)
0	863.457	858.316	0.059	863.528	0.002	858.316	0.060	863.166	0.003
716	868.150	872.387	0.049	870.268	0.024	872.387	0.049	870.397	0.026
964	871.390	872.387	0.011	872.036	0.007	872.387	0.011	871.904	0.006
2249	878.720	886.457	0.088	879.590	0.010	886.457	0.088	880.134	0.016
2783	884.933	886.457	0.017	885.724	0.009	886.457	0.017	885.827	0.010
3499	890.593	886.457	0.046	890.346	0.003	886.457	0.046	890.456	0.002
4557	896.463	900.528	0.045	897.845	0.015	900.528	0.045	898.367	0.021
5090	900.873	900.528	0.004	901.487	0.007	900.528	0.004	901.954	0.012
Avg			0.040		0.010		0.040		0.012

Std=Standard deviation, Avg= Average of standard deviation

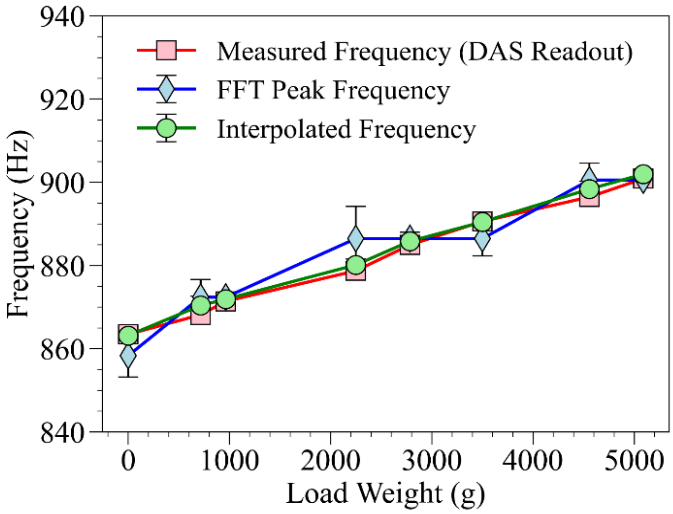

(a)

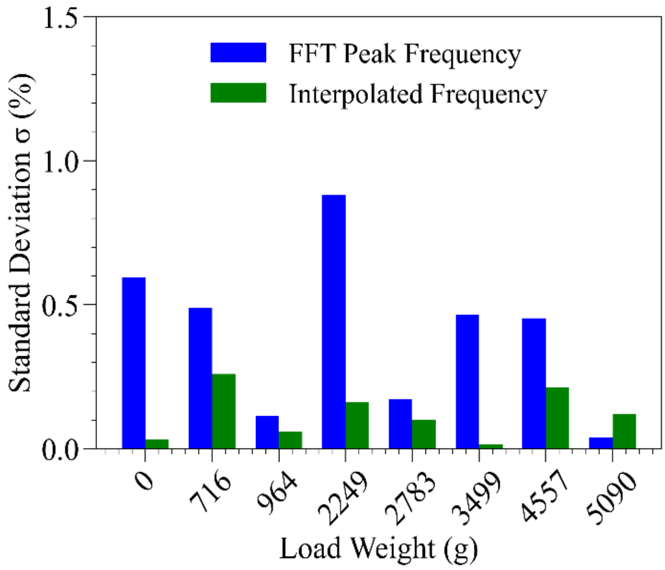

(b)

Fig. 12. Comparison of DAS readout, FFT peak, and interpolated frequencies using Square wave stimulus: (a) Resonant frequencies vs. Load weight; (b) Frequency deviation vs. Load weight

Fig. 11 illustrates the resonance frequency results and standard deviations obtained under sine wave stimulation. Fig. 11(a) compares the resonance frequencies measured by DAS readout; calculated FFT peak frequency and parabolic interpolation—across load levels ranging from 0 g to 5090 g. The results indicate a near-linear increase in resonance frequency from approximately 860 Hz to 900 Hz as the applied load increases. Both the DAS readout and the parabolic interpolation yield closely matching results with minimal error, whereas the FFT peak frequency shows greater fluctuations and higher deviations, particularly at load levels of 0 g, 716 g, 2249 g, 3499 g, and 4557 g. These discrepancies may arise from harmonics, mode coupling, or noise, which can distort FFT-based frequency detection under specific loading conditions. Fig. 11(b) presents the standard deviation of frequency differences between the FFT and parabolic interpolation methods, using the DAS readout as the reference. The standard deviation ranges from 0% to 1%, with the majority of values falling below 0.6%. The interpolated frequency based parabolic method results consistently align with the DAS values, with errors mostly under 0.3%. In contrast, the FFT-based results exhibit greater variability, with most errors exceeding 0.3%. At load levels of 964 g, 2783 g, and 5090 g, the frequency deviations between the two methods are minimal (below 0.5%), indicating high consistency. However, at the intermediate load of 2249 g, the FFT peak frequency exhibits a significant error peak of 1.5%, likely due to mode coupling or harmonic interference. This may reflect increased signal complexity under higher loading, which hinders accurate peak detection via FFT—especially when the signal is affected by noise or nonlinear vibration. At higher loads such as 3499 g and 4557 g, FFT errors remain relatively elevated (~0.5%), while the parabolic interpolation method continues to maintain low deviation, typically below 0.3%.

Fig. 12 presents the resonance frequency results and standard deviations for square wave stimulus. In Fig. 12(a), the resonance frequency trends show high consistency across the three measurement methods but there are some notable differences. Specifically, the DAS readout and the parabolic interpolation method produce closely matching values across all load levels, with differences typically less than 5 Hz. This consistency demonstrates the high reliability and suitability of both methods for identifying resonance frequency under square wave stimulation. In contrast, the FFT peak frequency method generally yields slightly lower resonance frequencies, particularly at intermediate load levels around 2000 g and 4000 g, where discrepancies can reach up to 10 Hz. This deviation may be attributed to the nature of FFT, which identifies the dominant peak in the frequency spectrum. Fig. 12(b) analyzes the frequency deviation between FFT and interpolated frequencies, using the DAS readout as a reference. The deviations range from 0% to 1%, with most values falling below 1%. At load levels of 964 g, 2783 g, and 5090 g, deviations between the two methods are minimal (below 0.3%), indicating a high degree of agreement. However, FFT peak frequencies exhibit greater errors at intermediate and higher load levels, with the largest deviation reaching 1% at 2249 g. In contrast, the parabolic interpolation method consistently maintains smaller errors—mostly under 0.3%—highlighting its superior accuracy under the complex spectral conditions introduced by square wave excitation.

Following Figs. 11 and 12, the parabolic interpolation method demonstrates maximum deviation below 0.3%. Specifically, it yields very small errors and provides resonance frequency values that closely match the reference values from the DAS readout under both sine and square wave stimuli. Owing to its high accuracy and consistency across various loading conditions, the parabolic interpolation method is selected as the primary approach for computing precise microstrain values in this study.

Based on the resonance frequency determined for each loading level, the precise microstrain can be calculated using the calibration relationship provided in the GV-2405 sensor specification. Therefore, the linear relationship between the resonance frequency f (Hz) and the strain ε (microstrain) is expressed as:

$$\varepsilon = K \times B \times \left(F_i^2 - F_0^2\right) \times 10^{-3} \qquad (10)$$

where K=4.062 is strain gage factor of the vibrating wire sensor and B=0.9838 is average batch calibration gage factor, as reported in the calibration certificate of the GV-2405 sensor [11]. In addition, F_i and F_0 are resonant frequency at current loading state and initial unloaded condition, respectively.

Since the GV-2405 sensor has a range of measured values up to 3300 microstrain [11], the linearity (%FS) must be calculated to evaluate the accuracy of the measurement methods. The linearity value is determined using the following equation:

$$\text{Linearity} = \frac{\varepsilon_m - \varepsilon_p}{FS} \times 100 \qquad (11)$$

where: ε_m and ε_p represent the measured and ideal linear values, respectively. FS denotes the full-scale measurement range of the sensor; according to the calibration report provided by the manufacturer of the GV-2405 sensor, FS is equal to 3300 microstrain [11].

The precise strain results obtained from the DAS readout, sine wave stimulus, and square wave stimulus methods are summarized in Table 2.

Fig. 13 compares the sensor's performance when using two types of excitation signals—sine wave and square wave—while also referencing direct measurements from the DAS readout. Fig. 13(a) illustrates the relationship between precise microstrain and applied load, while Fig. 13(b) analyzes the linearity error at specific load levels.

Table 2. Statistical analysis of microstrains and linearity errors

Load weigth (g)	Linear fit microstrain	DAS readout		Sine wave stimulus		Square wave stimulus	
		ε	%FS	ε	%FS	ε	%FS
716	40.826	32.523	0.257	46.699	0.172	50.092	0.275
964	53.722	55.046	0.032	59.005	0.152	60.585	0.200
2249	120.542	106.404	0.447	111.884	0.281	118.206	0.089
2783	148.310	150.102	0.031	155.154	0.185	158.383	0.282
3499	185.542	190.261	0.114	187.957	0.044	191.242	0.144
4557	240.558	232.181	0.291	241.546	0.007	247.789	0.182
5090	268.274	263.856	0.176	267.733	0.058	273.596	0.119
Average of %FS			0.193		0.129		0.185

%FS = % Full sacle, FS = 3300 microstrain following GV-2405 calibration report

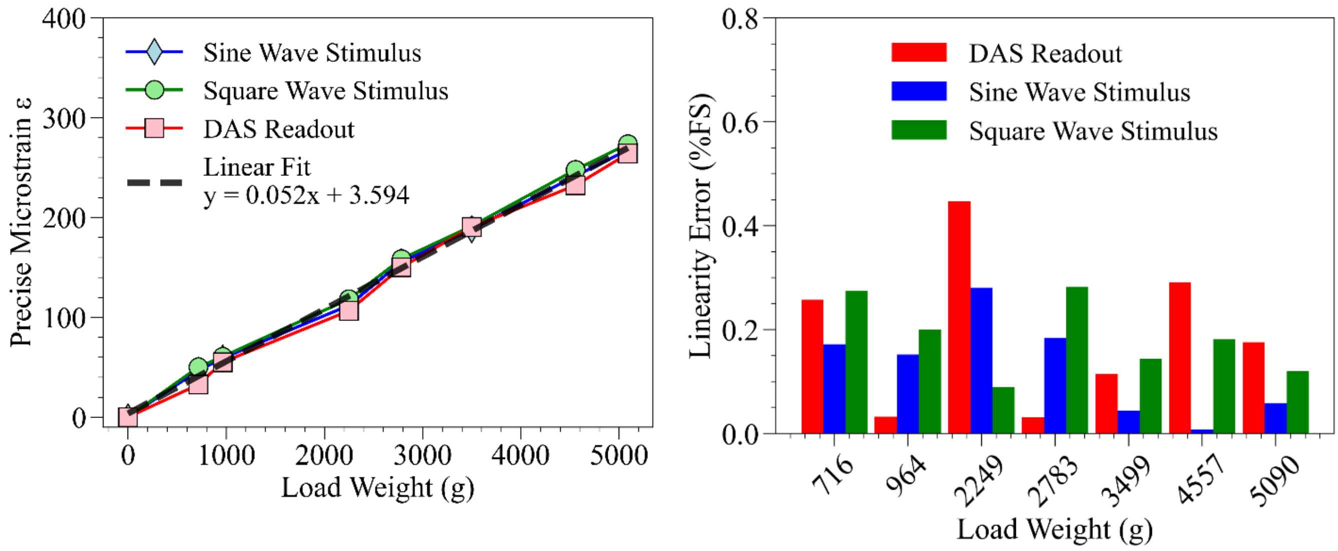

(a) (b)

Fig. 13. Comparison of Sine wave and Square wave stimuli and DAS readout: (a) Precise microstrain vs. Load weight; (b) Linearity vs. Load weight

In Fig. 13(a), precise microstrain increases linearly from 0 microstrain at 0 g to approximately 350 microstrain at 5090 g, with all cases including: DAS readout, sine wave, and square wave, showing consistent trends.

A linear regression line is included, defined by the equation y = 0.052x + 3.594, where y represents strain (in microstrain) and *x* represents load (in grams). The slope of 0.052 indicates that strain increases by approximately 52 microstrain per 1000 g of load, while the intercept of 3.594 microstrain at 0 g may reflect an initial offset or residual strain in the system. The measured values from DAS readout, sine and square wave stimuli are closely aligned across all load levels, with deviations typically below 10 microstrain. This demonstrates that both excitation methods accurately capture strain variations, and the DAS readout provides a reliable reference for comparison. The observed linear trend in strain aligns with fundamental mechanical principles, where strain is directly proportional to load in a beam under bending.

Fig. 13(b) presents the sensor's linearity error, expressed as a percentage of full scale (%FS), at load levels of 716 g, 964 g, 2249 g, 2783 g, 3499 g, 4557 g, and 5090 g. Linearity error is calculated by comparing actual strain values with ideal values derived from the linear regression in Fig. 13(a). Results show that linearity error ranges from 0% to approximately 0.5% FS, with the highest error observed at 2249 g. At lower load levels (716 g and 964 g), all three methods show minimal linearity errors below 0.3% FS, indicating excellent linear response under light loading. However, at the mid-range load (2249 g), the linearity error increases significantly, with the DAS readout showing the highest error (0.447% FS), while sine and square wave methods exhibit lower errors of 0.281% FS and 0.089% FS, respectively. This increase may be attributed to nonlinear behaviors in the vibrating system, such as variations in wire stiffness or non-uniform elongation under load. At higher loads (3499 g, 4557 g, and 5090 g), linearity errors decrease again, falling below 0.3% FS for all methods, suggesting a more stable system response under higher stress.

Notably, there are differences among the cases: the DAS readout generally yields higher linearity errors compared to the sine and square wave stimuli. The sine wave stimulus achieves the lowest average linearity error at 0.129%, while the DAS readout and square wave stimulus produce slightly higher errors of 0.193% and 0.185%, respectively. These results suggest that the sine wave stimuation method offers greater stability and accuracy.

6. Conclusion

This study presents the development of DUT Vibro vibrating wire sensor readout entirely developed by a Vietnamese research team as part of a domestic innovation initiative. The authors evaluated the performance of resonance frequency detection methods applied to vibrating wire sensors, utilizing sine wave and square wave excitation signals. These methods were assessed to determine their accuracy in precise microstrain measurement and the linearity of the sensing system.

Key findings of the study include:

1. The resonance frequency determined using the parabolic interpolation using three points method yielded the lowest error, closely matching the reference values obtained from the DAS readout, and demonstrated stable performance at both low and high load levels.
2. The FFT-based method exhibited greater variability in error, particularly at medium load levels (e.g., 2249 g), due to the influence of noise and nonlinear characteristics in the response signal.
3. Measured resonant frequency of steel wire using sine wave stimulation method produced more accurate results than square wave stimulation method.
4. The linearity error of the measurement system remained within the range of 0% to below 0.5% of full scale (FS). The combination of parabolic interpolation with sine wave excitation produced the lowest average linearity error (0.129% FS), confirming its suitability for high-precision strain measurement applications.
5. The linear regression analysis showed a strong fit (slope ≈ 0.052), indicating a linear relationship between the applied load and the measured strain.

Based on these results, the parabolic interpolation method using three points has been integrated into the DUT-Vibro vibrating wire readout system to ensure high accuracy in strain calculation, particularly in applications requiring minimal and stable error under varying loads. Although the experimental results demonstrate high accuracy under laboratory conditions, the study remains limited by the lack of field validation and a relatively narrow load range. Future work will focus on field testing, enhancing frequency resolution, and integrating noise-filtering algorithms to improve system stability and real-world applicability. This work contributes to the advancement of high-precision vibrating wire sensing systems and supports the broader goal of self-reliant sensor development in structural health monitoring.

Acknowledgments

This work was supported by The University of Danang – University of Science and Technology (DUT) grant funded by the Murata Science and Education Foundation (MSF) (No. 24VD09).

References

[1] J. Dunnicliff. (1988). Geotechnical instrumentation for monitoring field performance. *3rd ed. Wiley: New York.*

[2] T.P. Trinh, H.V. Tran, H.V. Cu, P.T. Nguyen, S.H. Nguyen, N.H.T. Vu, T.N. Nguyen. (2021). Study on monitoring stress-deformation of large-span arch bridges during construction using vibrating wire sensor systems in Vietnam (in Vietnam). *Journal of Science and Technology in Civil Engineering*, 15, 13-25. https://doi.org/10.31814/stce.huce(nuce)2021-15(7V)-02

[3] J.H. Zhao, F.F. Zhou, S.Y. Mao. (2014). Improvement and design of single coil vibrating-wire sensor signal acquisition system based on STM32. *Applied Mechanics and Materials*, 511-512, 764-769. https://doi.org/10.4028/www.scientific.net/AMM.511-512.764

[4] Z. Hua-Ling, Z. Xin-Yin. (2014). The high precision vibration signal data acquisition system based on the STM32. *Sensors & Transducers*, 172(6), 98-104.

[5] B. Mei, J. Lucas, S. Holé, I. Lamarque, N. Chéron. (2016). Excitation mode influence on vibrating wire sensor response. *Experimental Mechanics*, 56, 331-338. https://doi.org/10.1007/s11340-015-0101-6

[6] Q. Fu, B. Han. (2017). Bridge vibration monitoring system based on vibrating-wire sensor and ZigBee technologies. *2017 IEEE 9th International Conference on Communication Software and Networks (ICCSN 2017),* 338-342. doi: 10.1109/ICCSN.2017.8230131

[7] W. Tao, Z. Wenqian. (2019). A study on dynamic measurement methods based on vibrating wire sensors. *Measurement Science and Technology (MST)*, 30(2), 025105. DOI 10.1088/1361-6501/aaf8ff

[8] Y. Sang, Z. Zhang. (2020). Study on fast frequency-sweep method for vibrating wire sensor. *2020 IEEE International Conference on Artificial Intelligence and Computer Applications (ICAICA 2020)*, 409-413. doi: 10.1109/ICAICA50127.2020.9182514

[9] Z. Hou, L. Bao. (2023). Research and design of bridge distributed monitoring system based on LoRa technology. *IET Wireless Sensor Systems*, 13(3), 91-103. https://doi.org/10.1049/wss2.12059

[10] S. Lennart Johnsson, R.L. Krawitz. (1992). Cooley-Tukey FFT on the Connection Machine. *Parallel Computing*, 18(11), 1201-1221. https://doi.org/10.1016/0167-8191(92)90066-G

[11] Geovan. (2025). Vibrating wire strain gauge technology. Expert Edition. DONG-A GEOVAN. https://www.geovan.com/en/geotechnical_instruments/strain-gauge/ (accessed 10/04/2025).

[12] L.X. Le, B.X. Luong, Q.V. Ha, T.B. Phung. (2025). Cable tension estimation by Rayleigh's method considering restraint boundary conditions. *Journal of Science and Transport Technology*, 5(1), 92-103. https://doi.org/10.58845/jstt.utt.2025.en.5.1.92-103

[13] STMicroelectronics. (2025). STM32F103C8 Product overview. https://www.st.com/en/microcontrollers-microprocessors/stm32f103c8.html (accessed

10/04/2025).
[14] Digital Advanced Sensors (DAS). (2025). Digital Protractor: DIGIANGLE-1D/2D.
[15] V.D. Le. (2025). DUT Vibro Video. Mendeley Data, V1. doi: 10.17632/h9r7t3gmpc.1